BIOCHEMISTRY
including biophysical chemistry & molecular biology

Article

pubs.acs.org/biochemistry

Concurrent Cooperativity and Substrate Inhibition in the Epoxidation of Carbamazepine by Cytochrome P450 3A4 Active Site Mutants Inspired by Molecular Dynamics Simulations

Christian S. Müller,[†,‡] Tim Knehans,[§] Dmitri R. Davydov,[*,∥,⊥] Patricia L. Bounds,[‡] Ursula von Mandach,[†] James R. Halpert,[∥] Amedeo Caflisch,[*,§] and Willem H. Koppenol[*,‡]

[†]Department of Obstetrics, University Hospital Zurich, Zürich, Switzerland

[‡]Institute of Inorganic Chemistry, Swiss Federal Institute of Technology (ETH) Zurich, CH-8093 Zürich, Switzerland

[§]Department of Biochemistry, University of Zurich, CH-8057 Zürich, Switzerland

[∥]Skaggs School of Pharmacy and Pharmaceutical Sciences, University of California at San Diego, La Jolla, California 92093-0202, United States

[⊥]V. N. Orekhovich Institute of Biomedical Chemistry, Russian Academy of Medical Sciences, Moscow, Russia

Supporting Information

ABSTRACT: Cytochrome P450 3A4 (CYP3A4) is the major human P450 responsible for the metabolism of carbamazepine (CBZ). To explore the mechanisms of interactions of CYP3A4 with this anticonvulsive drug, we carried out multiple molecular dynamics (MD) simulations, starting with the complex of CYP3A4 manually docked with CBZ. On the basis of these simulations, we engineered CYP3A4 mutants I369F, I369L, A370V, and A370L, in which the productive binding orientation was expected to be stabilized, thus leading to increased turnover of CBZ to the 10,11-epoxide product. In addition, we generated CYP3A4 mutant S119A as a control construct with putative destabilization of the productive binding pose. Evaluation of the kinetics profiles of CBZ epoxidation demonstrate that CYP3A4-containing bacterial membranes (bactosomes) as well as purified CYP3A4 (wild-type and mutants I369L/F) exhibit substrate inhibition in reconstituted systems. In contrast, mutants S119A and A370V/L exhibit S-shaped profiles that are indicative of homotropic cooperativity. MD simulations with two to four CBZ molecules provide evidence that the substrate-binding pocket of CYP3A4 can accommodate more than one molecule of CBZ. Analysis of the kinetics profiles of CBZ metabolism with a model that combines the formalism of the Hill equation with an allowance for substrate inhibition demonstrates that the mechanism of interactions of CBZ with CYP3A4 involves multiple substrate-binding events (most likely three). Despite the retention of the multisite binding mechanism in the mutants, functional manifestations reveal an exquisite sensitivity to even minor structural changes in the binding pocket that are introduced by conservative substitutions such as I369F, I369L, and A370V.

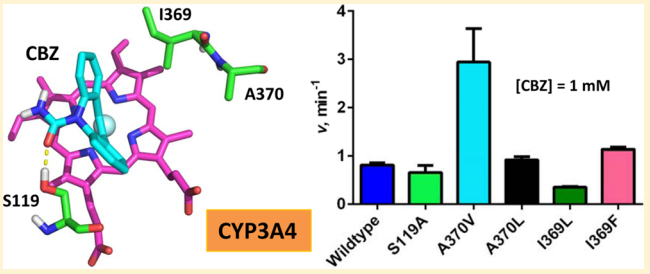

Cytochrome P450 3A4 (CYP3A4) is the most abundant cytochrome P450 enzyme in the liver of most adult humans.[1] This enzyme, which metabolizes about 50% of drugs on the market,[2] is the main hepatic cytochrome P450 involved in the metabolism of 5*H*-dibenzo[*b*,*f*]azepine-5-carboxamide (carbamazepine or CBZ). CBZ is a commonly prescribed anticonvulsive drug; its major metabolite is carbamazepine-10,11-epoxide (Figure 1).[3,4]

Numerous studies on *in vitro* CBZ epoxide formation that include data from incubations with human liver microsomes (HLM),[4−8] recombinant enzyme expressed as microsomes from insect cells,[9,10] and reconstituted purified enzyme preparations[4,11,12] have been published: both hyperbolic and sigmoidal dependencies of the reaction rate on the substrate concentration have been observed. Differing degrees of homotropic cooperativity have been reported for HLM[4,5,7,8] and microsomes from recombinant insect cells expressing human CYP3A4[6,9] that exhibit sigmoidal profiles. Michaelis−Menten kinetics[4] as well as sigmoidal profiles[7] have been reported for purified and reconstituted CYP3A4. The apparent

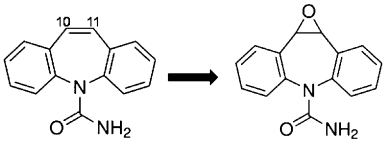

Figure 1. Structures of carbamazepine (left) and the major product of its CYP3A4-dependent oxidation, carbamazepine-10,11-epoxide (right).

Received: September 16, 2014
Revised: December 3, 2014
Published: December 29, 2014

DOI: 10.1021/bi5011656
Biochemistry 2015, 54, 711−721

inconsistency among these reports demonstrates that epoxidation of CBZ by CYP3A4 is very sensitive to both the experimental conditions and the enzyme source. Such inconsistencies in kinetics profiles have also been reported for other substrates, such as amitriptyline, nifedipine, and testosterone.[13] CBZ qualifies as a narrow therapeutic index drug,[14] of which the target for plasma concentration is 17−70 μM.[7] Because failure to maintain the target plasma range may cause toxic side effects, continuous therapeutic monitoring is desirable for optimal outcome of CBZ therapies. A potential approach to continuous monitoring is to use biosensors constructed from electrodes with immobilized P450 enzymes that can detect drug substrates such as CBZ.[15−17]

In this study, we sought to explore the mechanism of interaction of CYP3A4 with CBZ by engineering CYP3A4 variants with enhanced affinity for CBZ and/or increased epoxidation turnover. These studies were aimed at the elaboration of a CYP3A4-based electrochemical biosensor with improved capacity for determining CBZ concentration in clinical samples. Our approach to the optimization of CYP3A4 for CBZ binding encompasses explicit solvent molecular dynamics (MD) simulations of the structure of the CYP3A4 complex with CBZ in combination with site-specific protein engineering to incorporate amino acid alterations in the enzyme's active site. On the basis of our MD simulations, we designed four CYP3A4 mutants, each with putative stabilization of the CBZ molecule in a predicted productive binding mode that was aimed at increased affinity for CBZ and increased turnover of the epoxide product. We also constructed mutant S119A, which putatively disrupts a critical hydrogen bond, as a negative control with which we expected diminished turnover of the epoxide product.

The chosen mutants were cloned, expressed, and purified, and kinetics parameters of CYP3A4-dependent oxidation of CBZ were studied in a soluble reconstituted system. Significant effects of minor structural changes in the binding pocket of the enzyme, caused by the substitutions S119A, I369L, I369F, A370L, and A370V, were observed, demonstrating a profound sensitivity of both the enzyme−substrate binding interactions and the catalytic efficiency of CYP3A4. The observation of both homotropic cooperativity and substrate inhibition in the kinetics of CBZ epoxidation by wild-type and mutant CYP3A4 suggests that the interactions of the enzyme with the drug involve the binding to the enzyme of at least two, but more likely three, CBZ molecules. This conclusion is supported by multiple MD simulations that demonstrate the possible accommodation of multiple CBZ molecules in the CYP3A4 binding pocket.

MATERIALS AND METHODS

Reagents. CBZ was purchased from Acros Organics (Thermo Fisher Scientific, Waltham, MA, USA). L-α-Phosphatidyl choline, L-α-phosphatidyl ethanolamine, and L-α-phosphatidic acid were purchased from Avanti Polar Lipids (Alabaster, AL, USA). 3-[(3-Cholamidopropyl)-dimethylammonio]-1-propansulfonate (CHAPS) was purchased from Applichem GmbH (Darmstadt, Germany). HisPur Ni−NTA beads were obtained from Thermo Fisher Scientific, and CM macroprep ion-exchange support was obtained from Biorad (Hercules, CA, USA). *Escherichia coli* HMS 174 (DE3) cells were purchased from Merck, Darmstadt, Germany. Carbamazepine-10,11-epoxide, DEAE−sepharose fast-flow ion-exchange and adenosine 2′,5′-diphosphate agarose affinity supports were obtained from Sigma-Aldrich (St. Louis, MO, USA). Primers for recombinant DNA manipulations were obtained from Microsynth (Balgach, Switzerland). 10-Methoxy-carbamazepine was obtained from TLC PharmaChem (Vaughan, Ontario, Canada). Bactosomes with a high reductase/CYP3A4 ratio (Human CYP3A4R EasyCYP Bactosomes) were purchased from CYPEX, Ltd. (Dundee, U.K.).

Computational Methods. *Molecular Dynamics Simulations.* The simulations were carried out with the coordinates extracted from the structure of the CYP3A4 complex with metyrapone (Protein Data Bank (PDB): 1W0G).[18] CBZ was superimposed onto the bound structure of metyrapone, and water molecules, ions, and the metyrapone molecule were removed. Because of a lack of crystallographic density in the flexible segments, spurious N and C termini were neutralized with acetyl groups at Asp270 and Ala289 and *N*-methyl-amide groups at Glu262 and Ile276, whereas the natural termini were considered charged. Missing side-chain atoms were added with CHARMM.[19] Parameters for CYP3A4 and HEME were derived from the CHARMM27 force field.[20] The partial charges of the Cys442 side-chain thiolate were set as developed by Foloppe et al.[21] CBZ was parametrized according to the CHARMM general force field[22] and Paramchem.[23,24]

To determine the modes of binding of CBZ to CYP3A4, five independent MD simulations of 50 ns each were carried out with GROMACS (version 4.5.6).[25] First, the CYP3A4−CBZ complex was placed in a dodecahedral box, the size of which was set with a margin of at least 13 Å from any atom of the complex. The box was then filled with pre-equilibrated TIP3P water molecules,[26] and the system was neutralized with Na^+ and Cl^- ions at a concentration of 150 mM. Van der Waals and short-range electrostatic interactions were calculated up to a cutoff of 10 Å. Long-range electrostatics were evaluated with the particle mesh Ewald method,[27] and periodic boundary conditions were applied. All bonds involving hydrogen atoms were constrained by the LINCS algorithm,[28] and a 2 fs time step was used. The temperature was kept constant at 310 K by means of the velocity-rescaling algorithm implemented[29] in GROMACS, and the pressure was kept constant at 1 atm with a Parinello Raman barostat.[30,31] Mutations at the respective residue indices were introduced by simple remodeling in PyMOL.[32] For the simulations with multiple copies of CBZ bound, the starting positions were generated by manually positioning two, three, or four molecules of CBZ in the active site so that no steric clashes were introduced. All systems were energy minimized for 10 000 steps of the conjugate gradient algorithm before starting the MD. Subsequently, the system was equilibrated in an NPT simulation for 1 ns. From the resulting atomic positions, the production runs were started with different random seeds for the initial assignment of the velocities.

Clustering. The WORDOM[33] (version 0.22) implementation of the leader algorithm was used to cluster the snapshots saved along the MD trajectories by a criterion that was based on the root-mean-square deviation (RMSD) of the CBZ non-hydrogen atoms. Only the last 10 ns of each 50 ns run were used for clustering, i.e., the first 40 ns of each run were considered equilibration. First, the CYP3A4 Cα atoms were used to overlap the structures of the coordinate sets in the five 10 ns segments with the X-ray structure. Starting from one of the snapshots at 40 ns, which was taken as the first cluster, the leader algorithm proceeded iteratively by comparing each snapshot with the representative of the previously defined

DOI: 10.1021/bi5011656
Biochemistry 2015, 54, 711−721

clusters. A snapshot was assigned to a cluster if the RMSD was smaller than a threshold value of 2 Å. Simulations with two CBZ molecules positioned in the active site were clustered with a tree-based algorithm as provided in CAMPARI.[34,35] RMSD-based clustering over the entire 200 ns was carried out for each of the two CBZ molecules separately with a threshold radius (CRADIUS) of 2 Å, a tree height (BIRCHHEIGHT) of 16, and a coarsest threshold (CMAXRAD) of 10 Å. CYP3A4 Cα atoms were aligned before clustering. All figures were prepared with the PyMOL package.[32]

Experimental Section. *Recombinant DNA Manipulations.* Construct pSE3A4, expressing an N-terminally modified human P450 3A4 with a tetra-histidine tag attached at the C-terminus, was described previously.[36] Site-directed mutagenesis was carried out by means of PCR with the QuikChange Site-Directed Mutagenesis Kit (Agilent Technologies, Stratagene Products Division, La Jolla, CA, USA.).

Expression and Purification of CYP3A4 and P450 Reductase. Freshly transformed *E. coli* Topp3 cells were induced with 0.5 mM IPTG, and the CYP3A4 construct was expressed for 48−72 h before cells were lysed by sonication; expression levels were quantified by reduced CO binding.[37] The enzyme was purified from solubilized membranes via nickel-affinity chromatography on Ni−NTA beads and anion-exchange chromatography with CM macroprep ion-exchange support as described previously.[38,39] Recombinant NADPH cytochrome P450 reductase (CYPOR) from rat liver was expressed in *E. coli* Topp3 cells and was purified as described previously.[36] The purity of the enzymes was analyzed via SDS−polyacrylamide gel electrophoresis and absorbance spectroscopy.

Absorbance Spectroscopy and Analysis of the Spectra. The spectra were recorded at 28 °C with a Specord S 250 UV−vis spectrophotometer equipped with a Peltier thermostat and a stirring device (Analytik Jena, Jena, Germany). The concentrations and the spin state of CYP3A4 were quantified on the basis of the approximation of the heme protein absorbance spectra with a set of the prototype absorbance spectra of CYP3A4's (Fe^{3+}) high-spin, low-spin, and P420 states.[40] The concentration of CYPOR was determined on the basis of the prototypic spectrum of the pure enzyme with an extinction coefficient equal to 21.4 mM^{-1} cm^{-1} at 456 nm.[41] In these calculations, the linear least-squares approximations of the spectra with combinations of the absorbance standards were carried out with the SpectraLab software package.[42]

Reconstitution of Wild-Type Recombinant CYP3A4 and Mutants. A functional mono-oxygenation system with CYP3A4 and CYPOR was reconstituted in a micellar system containing phospholipids added as chloroform solutions of L-α-phosphatidyl choline, L-α-phosphatidyl ethanolamine, and L-α-phosphatidic acid mixed at a molar ratio of 1:2:0.6, respectively,[39] as well as 0.4% CHAPS. The pellet of phospholipids obtained after removal of the solvent under a flow of argon gas was then resuspended in buffer A (100 mM HEPES, 150 mM KCl, 0.5 mM EDTA, and 1 mM DTT, containing 10% *v*/*v* glycerol, pH 7.4) to a final concentration of 10 mg mL^{-1} (13.3 mM) by vigorous shaking on a vortex mixer. The resulting suspension was then homogenized by extrusion through a 200 nm pore-size filter with an Avanti miniextruder (Avanti Polar Lipids, Alabaster, AL, USA.). A mixture of CYP3A4 and CYPOR containing 10 μM of each protein was then supplemented with the 6.5 mM phospholipid suspension to an final concentration of 1.5 mM, and buffer A (1.5% CHAPS) was added to a final concentration of 0.4% CHAPS. The mixtures were incubated overnight at 4 °C under continuous shaking in a table-top thermomixer (Eppendorf, Hamburg, Germany). The reproducibility of the procedure with overnight incubation was considerably better than that with 30 min incubation, and subsequent activity measurements showed no decrease in activity of the reconstituted enzyme after overnight compared to that of after 30 min of shaking.

Kinetics Assay: Formation of Carbamazepine-10,11-epoxide. Reactions were carried out at 37 °C in microreaction tubes in a table-top shaker. The reconstituted enzymes were diluted 20-fold into buffer (0.1 M HEPES, pH 7.4). The final concentrations of CYP3A4 and CYPOR were 0.5 μM, except for the incubations involving CYP3A4 bactosomes, in which the final concentrations were 0.05 μM. The working concentration of CHAPS was 0.02% (325 μM). CBZ was added from methanol stock solutions for a final methanol concentration of 1%, and addition of 20 μL of a 5× NADPH regeneration system containing 25 mM glucose-6-phosphate (GSP), 5 U/mL glucose-6-phosphate dehydrogenase (GSPDH), and 5 mM $NADP^+$ in 50 mM potassium phosphate buffer (pH 7.4) brought the reaction volume to 100 μL and the final concentrations of the regeneration system components to 5 mM, 1 U/mL, and 1 mM, respectively. The reaction mixture was buffered at pH 7.4 with 75 mM HEPES and 10 mM potassium phosphate.

The linear ranges of product formation as a function of time were determined for each mutant by taking aliquots of the reaction mixture at 0, 5, 10, 15, 20, 25, and 30 min after initiation of the reaction. For most of the mutants, we obtained profiles for the increase in product concentration at the time points larger than 20 min that were linear; the exceptions were mutants S119A and I369F, for which the time dependence of product formation was linear for only ca. 15 min. Consequently, incubations were carried out for 20 min for incubations with wild-type CYP3A4 and mutants I369L and A370V/L and for 15 min with mutants S119A and I369F. All incubations were conducted in triplicate. The enzymatic reactions were stopped by adding an equal amount of ice-cold methanol containing 20 μM of the internal standard 10-methoxy-carbamazepine, followed by 1:1 dilution with deionized water for a final methanol concentration of 25%. The samples were analyzed by reversed-phase HPLC on a Ultimate 3000 system (Thermo Fisher Scientific, Reinach, Switzerland) on a 150 mm × 4.5 mm diameter Gravity C18 column (Macherey-Nagel GmBH & Co. KG, Düren, Germany) with 30:70 acetonitrile/water containing 0.1% formic acid as the mobile phase.

The rates of reactions as a function of substrate concentration were fit to either the regular Hill equation or the Hill equation complemented with an allowance for partial substrate inhibition, as described in the Supporting Information, by means of a combination of the Nelder−Mead and Marquardt nonlinear regression algorithms, as implemented in the SpectraLab software package.[42]

RESULTS

CBZ Epoxidation by CYP3A4-Containing Bactosomes. In good agreement with previous studies of CYP3A4-dependent metabolism of CBZ, we detected no product in significant amounts except for carbamazepine-10,11-epoxide.[4] Upon examination of the substrate-concentration dependence of the kinetics profiles, we extended the range of CBZ

DOI: 10.1021/bi5011656
Biochemistry 2015, 54, 711−721

concentrations used in our analyses to 0−2000 μM, a considerably larger concentration range than that reported in previous studies.[4−6,9] The kinetics profile reveals moderate but clearly pronounced substrate inhibition that becomes evident at CBZ concentrations >700 μM (Figure 2). The fit of the initial

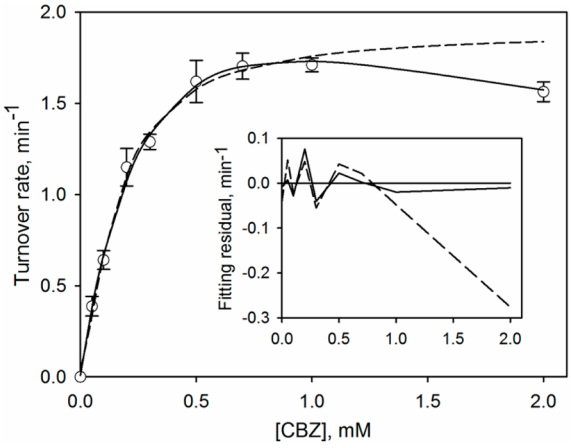

Figure 2. Substrate dependence of the rate of formation of carbamazepine-10,11-epoxide catalyzed by recombinant CYP3A4 in bactosomes. Data points represent mean values from three individual measurements, and the error bars show the respective standard deviations. Results of fitting to the Hill equation (dashed line) and to eq 1 (solid line) are shown. The inset shows plots of the respective residuals.

parts of the titration curves ([CBZ] ≤ 1000 μM) with the Hill equation (Figure 2, dashed line) is consistent with positive cooperativity, with a Hill coefficient (h) of 1.4 ± 0.4 (S_{50} = 162 ± 4 μM, k_{cat} = 1.9 ± 0.3 min^{-1}); this is in agreement with a previous report in which CYP3A4-dependent epoxidation of CBZ was characterized as exhibiting inherent homotropic cooperativity with h = 1.4−1.7.[7]

However, the Hill equation fits of the titration curves are satisfactory only to a CBZ concentration of ca. 700 μM; at higher concentrations, there is evident systematic deviation of the experimental data from the equation curve (Figure 2, inset). In an attempt to achieve an appropriate approximation of the experimental data over the entire range of CBZ concentrations, we fit the data sets to the Michaelis−Menten equation adapted for partial substrate inhibition, expressed as

$$V_S = \frac{k_{cat}[E]_0[S](\alpha[S] + K_I)}{K_M K_I + [S](K_I + [S])} \quad (1)$$

where V_S and k_{cat} designate the reaction rate at substrate concentration $[S]$ and the apparent catalytic rate constant, respectively. The Michaelis−Menten constant and the dissociation constant of the enzyme complex with the inhibitory substrate molecule are designated as K_M and K_I respectively, and the coefficient α represents the fraction of k_{cat} that is retained in the inhibitory complex when a second molecule of substrate is bound. The derivation of this equation is described in the Supporting Information.

As shown in Figure 2 (solid line), the experimental data sets may be fit to eq 1 ($\rho^2 \geq 0.982$) with no systematic deviations over the entire range of CBZ concentrations studied (Figure 2, inset). The parameters for fitting eq 1, representing the averages of the results obtained in three individual experiments, are k_{cat} = 3.1 ± 0.5 min^{-1}, K_M = 140 ± 10 μM, K_I = 1.6 ± 0.3 mM, and α = 0.21 ± 0.08. Therefore, the data obtained with bactosomes are consistent with a model where the maximal rate of CBZ metabolism is obtained by the complex of CYP3A4 with one substrate molecule, and the subsequent low-affinity binding of a second CBZ molecule to this complex results in an ca. 5-fold decrease in the rate of CBZ metabolism. It appears probable, therefore, that earlier reports of positive cooperativity in CYP3A4-dependent CBZ metabolism should be questioned because the titration curves thought to fit the Hill equation (Figure 2, dashed line) were recorded over a range of CBZ concentrations too low to cause pronounced substrate inhibition.

Probing the CBZ Binding Mode to CYP3A4 with MD Simulations. According to the above analysis, we infer that the complex of CYP3A4 with one substrate molecule in the substrate-binding pocket may serve as an adequate initial model of the catalytically competent complex of the enzyme with CBZ. Thus, we selected a binary complex of CYP3A4 with one CBZ molecule as the subject for initial MD simulations aimed at eliciting the structure of the CBZ−CYP3A4 complex and the orientation of the substrate molecule in the active site.

Figure 3b shows the time series of the backbone RMSD from the X-ray structure of CYP3A4 (PDB: 1W0G),[18] which reaches

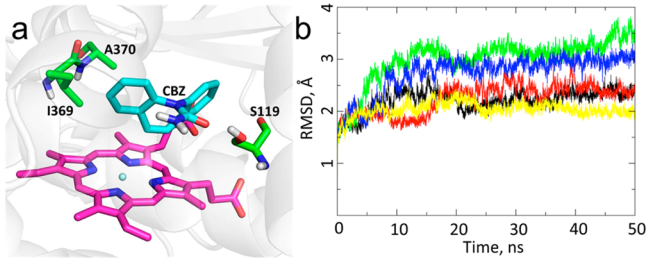

Figure 3. Results of MD simulations with the complex of wild-type CYP3A4 with one molecule of CBZ. (a) A representative snapshot of the most populated cluster. The residues selected for mutation (S119, I369, and A370), CBZ, and the heme group are shown with stick models in green, cyan, and magenta, respectively. The protein backbone is shown in transparent gray. (b) Time series of the RMSD from the crystal structure (PDB: 1W0G) of the protein backbone after alignment of Cα carbons. The RMSD reaches a plateau after about 20 ns in the five independent runs, each of which is plotted with a different color.

a plateau between 2 and 3 Å after about 10 ns (equilibration phase). We determined the binding modes of CBZ in five independent MD runs of 50 ns each, where only the last 10 ns of each run was evaluated. In the most populated, i.e., largest, cluster of the CBZ poses, the heme iron is located within 5 Å of the center of the bond between the carbon atoms 10 and 11 (C10,C11), which is compatible with the CYP3A4-catalyzed epoxidation of CBZ (Figure 3a). It should be noted, however, that the relevance of this binding mode to the actual mechanism of interactions is difficult to assess because it was primarily sampled in only one of five MD runs. The CBZ molecule that was initially superimposed at the position of the removed metyrapone did not exit the CYP3A4 binding site in any of the runs. On the basis of the binding mode of CBZ in the largest cluster of poses deduced from MD simulations (Figure 3a), we selected the amino acids S119, A370, and I369 as targets (Table S1). We suggested five single-point mutants on the basis of the mean distances between the center of mass (COM) of the respective residues and the COM of CBZ in this

DOI: 10.1021/bi5011656
Biochemistry 2015, 54, 711−721

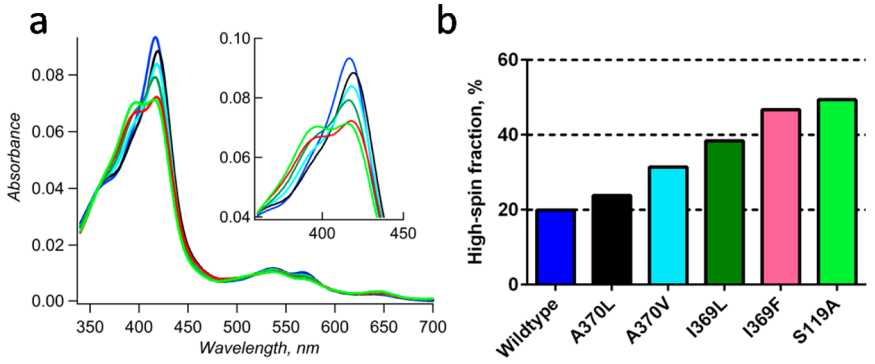

Figure 4. Effect of mutations on the spin state of purified CYP3A4 proteins. (a) Absorbance spectra of wild-type CYP3A4 (blue) and its mutants: I369F (red), I369L (green), S119A (light green), A370V (turquoise), and A370L (black). Spectra were normalized to correspond to a heme protein concentration of 1 μM. The inset shows the Soret band region of the same spectra. (b) Respective fraction of the high spin state of these heme proteins. Conditions: 100 mM HEPES, pH 7.4, 1 mM DTT, 10% *v*/*v* glycerol. The concentration of P450 was in the range of 1.5−2.5 μM.

cluster (Figure 3a). We predicted that mutants I369L, I369F, A370V, and A370L would lead to improved steric complementarity, i.e., Van der Waals interactions, between CYP3A4 and the 5*H*-dibenzo[*b*,*f*]azepine ring system of CBZ. Mutant S119A was selected as a negative control and was designed to disrupt the structural stability of the productive binding mode by eliminating the hydrogen bond between the carbonyl oxygen of CBZ and the S119 side-chain hydroxyl group.

Enzyme Expression, Purification, and Reconstitutions. On the basis of the results of the MD simulations, we elected to probe the effect of the mutations S119A, I369L, I369F, A370L, and A370V on the metabolism of CBZ by CYP3A4. Expression of all five constructs in *E. coli* provided stable P450 holoprotein, which is in good agreement with earlier reports on the expression and purification of mutants S119A,[43] A370V,[44] and I369F.[45] The yields of expression obtained with all of these mutants were generally somewhat lower than the yield of wild-type CYP3A4.

As seen from the absorbance spectra of the purified enzymes (Figure 4a), all five substitutions probed in this study caused a notable increase in the amplitude of the heme protein absorbance band at 396 nm relative to the amplitude of the band at 417 nm. This is indicative of a displacement of the spin equilibrium toward the ferric high-spin state. This displacement is most pronounced in mutants I369F and S119A, where the fraction of high-spin heme protein approaches 50%, in sharp contrast to the spin state of wild-type CYP3A4, where the high-spin fraction at 28 °C does not exceed 20% (Figure 4b).

Effect of Mutations on CYP3A4-Dependent Epoxidation of CBZ. In initial experiments, we assessed the turnover of CBZ epoxidation in the reconstituted system with the purified mutants and wild-type CYP3A4 (rCYP3A4) at apparent subsaturating (0.1 mM) and saturating (1 mM) concentrations of the substrate.

To analyze the effects of these substitutions in more detail, we evaluated broader kinetics profiles of wild-type CYP3A4 and mutants in reconstituted system, increasing the range of CBZ concentration studied up to 2 mM (Figure 5, Table 1). Although the overall quality of the fit of the titration curves obtained with wild-type CYP3A4 to the Hill equation (Figure 5, dashed line, and Table 1, h = 2.0 ± 0.9, S_{50} = 300 ± 100 μM, and k_{cat} = 1.0 ± 0.3 min^{-1}) appears acceptable (ρ^2 = 0.957), systematic deviations of the experimental points (Figure 5a, circles) suggest the presence of substrate inhibition at higher concentrations, similar to that observed with the CYP3A4-

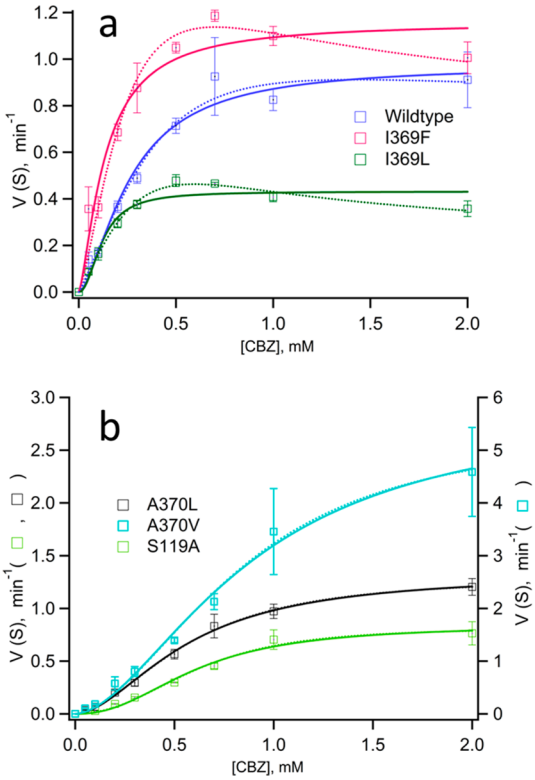

Figure 5. Substrate dependence of the rate of formation of carbamazepine-10,11-epoxide catalyzed by purified CYP3A4 and mutants in the reconstituted system. Incubations were carried out with 0.5 μM CYP3A4. Data points represent the mean values of three individual measurements, and the error bars show the respective standard deviations. Fits to the Hill equation (dashed line) and to eq 2 (solid line) are shown. (a) Plots obtained with wild-type CYP3A4 (circles) and the mutant enzymes I369F (squares) and I369L (triangles). (b) Plots obtained with mutants S119A (circles), A370V (squares), and A370L (triangles).

containing bactosomes. However, in the case of mutants I369F and I369L, the substrate inhibition is much more evident than with wild-type CYP3A4 (Figure 5a); mutants S119A, A370V, and A370L show no visible signs of substrate inhibition (Figure 5b). In contrast, the S-shaped kinetics profiles obtained with these mutants are indicative of a high degree of cooperativity.

To justify the apparent combination of the positive cooperativity and substrate inhibition mechanisms observed

DOI: 10.1021/bi5011656
Biochemistry 2015, 54, 711−721

Table 1. Parameters of CYP3A4-Dependent Epoxidation of Carbamazepine[a]

	Hill equation[b]				Hill equation complemented with substrate inhibition (eq 2)					
system	k_{cat}, min^{-1}	S_{50}, mM	h	ρ^2	k_{cat}, min^{-1}	S_{50}, mM	h	K_i, mM	α	ρ^2
bactosomes	1.9 ± 0.3	0.16 ± 0.04	1.4 ± 0.4	0.979	2.9 ± 0.7	0.3 ± 0.2	1.06 ± 0.08	1.3 ± 0.8	0.3 ± 0.3	0.991
rCYP3A4 w/t	0.9 ± 0.3	0.3 ± 0.1	2.0 ± 0.9	0.957	1.4 ± 0.4	0.50 ± 0.04	1.4 ± 0.4	0.79 ± 0.04	0.6 ± 0.5	0.964
rCYP3A4 I369L	0.42 ± 0.06	0.14 ± 0.02	1.80 ± 0.10	0.884	0.8 ± 0.4	0.3 ± 0.2	1.4 ± 0.3	1.1 ± 0.5	0.2 ± 0.1	0.989
rCYP3A4 I369F	1.4 ± 0.2	0.20 ± 0.07	1.3 ± 0.5	0.932	3 ± 1	0.6 ± 0.4	1.2 ± 0.3	1.1 ± 0.6	0.2 ± 0.4	0.971
rCYP3A4 S119A	0.8 ± 0.1	0.61 ± 0.07	2.5 ± 0.4	0.985	1.2 ± 0.1	0.94 ± 0.08	2.1 ± 0.3	1.0 ± 0.2	0.5 ± 0.1	0.990
rCYP3A4 A370V	5 ± 1	1.0 ± 0.3	2.1 ± 0.9	0.991	4.6 ± 0.9	1.1 ± 0.3	1.9 ± 0.6	5 ± 8	0.96 ± 0.07	0.991
rCYP3A4 A370L	1.3 ± 0.4	0.6 ± 0.3	2.0 ± 0.6	0.993	1.2 ± 0.2	0.77 ± 0.07	1.7 ± 0.2	5 ± 9	1.4 ± 0.7	0.993

[a]The values given in the table represent the averages of three individual measurements, and the values after ± show the confidence intervals calculated for $p = 0.05$. [b]In cases with clearly pronounced substrate inhibition (CYP3A4 bactosomes, reconstituted systems with mutants I369L and I369F), the fitting to the conventional form of the Hill equation was carried out with the data subsets corresponding to a CBZ concentration range of 0−1 mM. The square correlation coefficients given in the table correspond to the entire region of CBZ concentrations (0−2 mM) in all cases.

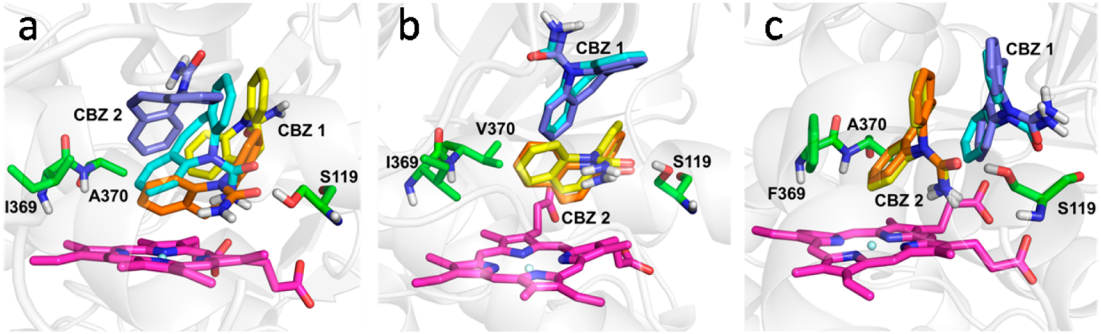

Figure 6. Results of MD simulations with the complex of two molecules of CBZ and (a) wild-type CYP3A4, (b) A370V, and (c) I369F. Each panel shows two representatives that correspond to the most populated clusters obtained with each of the two CBZ molecules for clustering. Clustering of the non-hydrogen atoms of the CBZ molecules was carried out upon structural alignment of all snapshots of the MD trajectories to the X-ray structure via the Cα atoms of the α-helical residues of CYP3A4. Only in panel a are the orientations of the CBZ molecules different, depending on which of the two CBZ molecules was subjected to clustering, indicating that the sampling did not converge.

in the mutants, we attempted to approximate the experimental data with an equation representing a combination of the Hill equation formalism with an allowance for substrate inhibition, represented as

$$V_S = \frac{k_{cat}\cdot[E]_0\cdot[S]^h\cdot(K_I + \alpha\cdot[S])}{S_{50}^h\cdot K_I + [S]^h\cdot(K_I + [S])} \quad (2)$$

The derivation of eq 2 is described in the Supporting Information. The S_{50} term in eq 2 is defined in a way similar to that in the regular Hill equation: as the hth root of the apparent dissociation constant of the catalytically competent enzyme−substrate complex. Where $h = 1$, eq 2 reduces to eq 1, and S_{50} is equivalent to K_M.

The fits of eq 2 to the data are shown in Figure 5 (solid lines), and the respective parameters are summarized in Table 1. Equation 2 clearly provides a better model for fitting data sets obtained with wild-type CYP3A4, whether prepared as bactosomes or as reconstituted systems, and with mutants I369L and I369F. For the data obtained with the mutants, the fit to eq 2 is as good as that to eq 1. The values obtained for the parameter α with mutants A370L and A370V are close to unity, which suggests that the binding of additional substrate molecules would not affect the activity of the enzyme; thus, we conclude that substrate inhibition is completely abolished in these mutants.

Analysis of the kinetics parameters suggests that, over the five mutations probed in this study, only the I369F substitution and, especially, the A370V substitution cause considerable increases in enzyme turnover with CBZ compared with wild-type (Table 1). In the case of I369F, the increase in the k_{cat} value is attenuated by enhanced substrate inhibition that is caused by a decrease in the fraction of activity retained in the inhibitory complex (α). However, for the A370V mutant, where substrate inhibition is eliminated, the increase in the CBZ turnover is substantial (Figure 5b, Table 1).

The clearly pronounced positive cooperativity in CBZ metabolism observed with mutants A370V, A370L, and S119A suggests that the formation of the catalytically competent complex with CBZ in these mutants requires the binding of at least two substrate molecules per molecule of the enzyme. At the same time, in contrast to mutants A370V and A370L, where substrate inhibition is eliminated, the fit of the data obtained with S119A to eq 2 indicates that the metabolism of CBZ by this mutant is characterized by a combination of a prominent positive cooperativity ($h = 2.1 \pm 0.3$) with a moderate degree of substrate inhibition ($\alpha = 0.5 \pm 0.1$); this further suggests that the mechanism of interaction with CBZ involves at least three separate substrate binding events.

MD Simulations of Two to Four CBZ Molecules in the CYP3A4 Binding Pocket. On the basis of the analysis of the kinetics profiles for CBZ metabolism, we concluded that

DOI: 10.1021/bi5011656
Biochemistry 2015, 54, 711−721

changes in CBZ metabolism caused by the mutations at positions 369, 370, and 119 cannot be accurately described by simulations with a single CBZ molecule bound. Therefore, we conducted MD simulations with two, three, or four CBZ molecules positioned in the CYP3A4 binding pocket. Five MD simulations each with two copies of CBZ in the active site were carried out with wild-type CYP3A4 and mutants I369F and A370V. Cluster analyses yielded nonidentical largest clusters for both mutants and wild-type. The simulation times of 0.2 μs per MD run, equal to a total sampling time of 1 μs for each of the three CYP3A4 variants, were intended to achieve convergent data. Importantly, similar to the single-CBZ simulations, the clusters obtained stem mainly from only one of the five runs, which is indicative of a lack of convergence. The largest clusters for each of wild-type CYP3A4 and mutants A370V and I369F are shown in Figure 6. Only for the A370V mutant (Figure 6b) is the binding mode, i.e., the position and orientation, of the CBZ closest to the heme essentially identical to that of the most populated cluster in the single-CBZ wild-type run with the C10−C11 bond close to the heme iron (Figure 3a). Interestingly, the hydrogen bond observed between S119 and the carbonyl oxygen of one CBZ molecule is retained in all panels in Figure 6, which further supports our hypothesis that S119 plays an important role in substrate binding.

Partial dissociation of a single CBZ molecule was observed in one of the multiple-CBZ MD simulations (Figures 7 and S1). Analysis of the unbinding pathway reveals that the CBZ molecule moves to the periphery of CYP3A4 through the F′-helix β-sheet-1 putative substrate-binding channel predicted by Williams et al.[18] To assess the ability of CYP3A4 to accommodate more than two CBZ molecules, we carried out five independent MD runs of 100 ns each with wild-type CYP3A4 plus three or four CBZ molecules (Figure S1). No dissociation events were observed, and the distance of the CBZ molecule furthest from the heme iron was never larger than 18 Å. These results indicate that the CYP3A4 binding pocket is large enough to accommodate up to four CBZ molecules and that the A370V and I369F mutations considerably affect the mobility of CBZ molecules bound in the binding pocket.

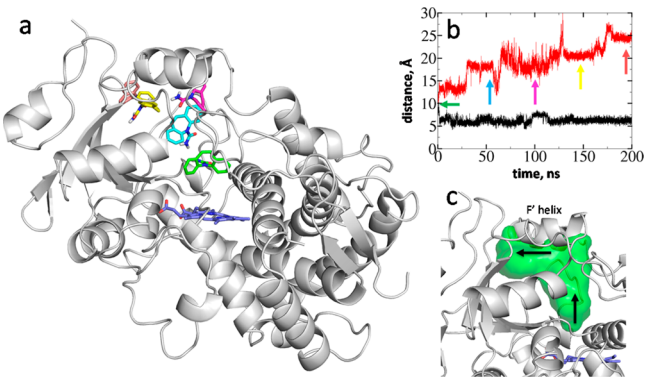

Figure 7. Pathway of egress from the heme pocket for one of the two bound CBZ molecules from wild-type CYP3A4 to a distance >20 Å from the heme iron. (a) Structure of CYP3A4 showing the positions of the CBZ molecule during its dissociation. The initial position of the CBZ molecule is highlighted in green and the positions after 50, 100, 150, and 200 ns are shown in cyan, magenta, yellow, and maroon, respectively. The second CBZ molecule is not shown. (b) Time series of the COM distance between CBZ C10,C11 and the heme iron. The distances of the bound CBZ molecule are shown in black, and the distances of the unbinding CBZ molecule are shown in colors corresponding to those used in panel a. The green arrow indicates the starting position of the molecule. (c) Surface circumscribed by the central nitrogen atom of the dissociating CBZ molecule over the course of a single 200 ns simulation. The protein backbone from the first snapshot of the simulation is shown in white and does not account for changes during the simulation. The arrows indicate the general direction of the movement of the CBZ molecule.

DISCUSSION

The present study represents the first attempt to employ MD simulations to produce CYP3A4 mutants with enhanced activity of epoxidation of carbamazepine combined with subsequent *in vitro* examination of the impact of the mutations on kinetics parameters. Our initial studies of the kinetics of CBZ epoxidation by CYP3A4-containing bactosomes reveal pronounced substrate inhibition, leading us to suggest that the apparent positive cooperativity reported in earlier studies of CBZ metabolism might be due to the limited range of substrate concentrations examined. We demonstrate that the kinetics profiles obtained with bactosomes adequately approximate the Michaelis−Menten equation complemented with an allowance for partial substrate inhibition (eq 1). The complex of CYP3A4 with one substrate molecule bound in the substrate-binding pocket (Figure 3) may be taken as a reasonable model of the catalytically competent complex.

In the MD simulations carried out with a single CBZ molecule, the most populated cluster displays a productive CBZ binding mode that is compatible with the epoxidation reaction. The distance between the COM of CBZ carbon atoms 10 and 11 to the heme iron is less than 5 Å. On the basis of the analysis of the structure in this cluster, we identified CYP3A4 mutations (I369L, I369F, A370V, and A370L) that could lead to improved steric complementarity via Van der Waals interactions of the enzyme with the three-ringed 5*H*-dibenzo[*b*,*f*]azepine system of CBZ. The S119A mutation was designed to abolish the hydrogen bond to the carboxyl function of CBZ to decrease the stability of the binding mode and, thus, the overall binding affinity.

Although the approach that was based on MD simulations with one CBZ molecule was successful in the case of mutants I369F and A370V, where the maximal rate of CBZ turnover is considerably increased, examination of the kinetics profiles of CBZ metabolism with the full series of mutants reveals certain limitations of this simplified model. We can best approximate the kinetics profiles obtained *in vitro* with wild-type CYP3A4 or mutants by means of a model that combines the positive cooperativity mechanism with an allowance for partial substrate inhibition (eq 2). According to our analysis with this model, marginal cooperativity (h = 1.2−1.4) is exhibited by wild-type CYP3A4 and mutants I369L and I369F, whereas the cooperativity is more clearly pronounced (h = 1.7−2.1) in mutants S119A, A370V, and A370L. Substrate inhibition is quite modest in wild-type CYP3A4 and the S119A mutant ($\alpha \approx$ 0.5) and eliminated in mutants A370V and A370L ($\alpha \approx 1$), but it is considerably enhanced in mutants I369L and I369F ($\alpha \approx$ 0.2). The complex mix of positive cooperativity and substrate inhibition in CBZ metabolism are consistent with the results of Egnell and co-workers,[7] who compared the kinetics profiles for CBZ epoxidation by HLM to those obtained with purified CYP3A4 in a reconstituted system and demonstrated that although data obtained with HLM are consistent with a two-site model where binding of the first CBZ molecule increases the

DOI: 10.1021/bi5011656
Biochemistry 2015, 54, 711−721

enzyme affinity for binding of a second substrate molecule the reconstituted system instead exhibits substrate inhibition.[7]

On the basis of our findings, we suggest that CYP3A4−CBZ interaction is best explained with a model that involves binding of three or more CBZ molecules in the active site. MD simulations of the complex of CYP3A4 with two to four CBZ molecules provide strong support for this suggestion; no complete egress of substrate was observed in five MD simulations involving three or four CBZ molecules. In the simulations where two molecules of CBZ are bound to wild-type CYP3A4 or mutants I369F or A370V (Figure 6), the most populated binding mode of the single-copy simulations of CBZ was observed only for A370V: in this case, one of the two CBZ molecules is bound in a putative catalytic pose. The finding that this pose appears to be stabilized by the second CBZ molecule provides a plausible explanation for homotropic cooperativity in CBZ epoxidation. Indeed, the A370V mutant is the only one of the three enzyme variants probed with simulations that exhibits prominent homotropic cooperativity (Figure 5, Table 1). However, given the limited sampling in the simulations, we caution that this observation may be coincidental.

In the 15 simulations of 2 CBZ molecules in the active site of CYP3A4 (5 simulations each with wild-type, A370V, and I369F), only one partial egress of substrate was observed: the case of wild-type CYP3A4 (Figure 7). We compared the cumulative volume of the dissociation trajectory of the CBZ undergoing partial dissociation via the sampled volume of the COM of C10/11 (Figure 7c) to the position of the substrate access channel predicted by Williams et al. on the basis of the X-ray structure (PDB: 1W0G) of CYP3A4[18] and found that the volumes largely match; hence, our simulation supports the geometry of the substrate- and solvent-accessible binding pocket of CYP3A4 previously proposed.

Although a multisite binding mechanism in mutants is retained, the enzyme is exquisitely sensitive to the minor structural changes in the binding pocket introduced by the point mutations S119A, I369F, I369L, A370L, and A370V. The observation of the hydrogen bond between the CBZ molecule adjacent to the heme and the S119 residue (Figure 6) provides a clue to the effects of the S119A substitution (Figure 4, Figure 5, Table 1). Importantly, this bond is found in the structures of all simulated variants (wild-type, A370V, and I369F). The absence of the stabilizing hydrogen bond in the S119A mutant may explain the reduced affinity of this mutant for CBZ. Further, enhancement of homotropic cooperativity in CBZ epoxidation by this mutation reveals an increased role for the binding of a second substrate molecule in stabilizing the catalytically competent complex. These results also support that residue S119 plays a key role in substrate binding in CYP3A4,[44,46−50] in agreement with a recent study in which it was shown that the association of CYP3A4 with ritonavir analogues, which do not engage in hydrogen bonding to S119, is facilitated by polar interactions mediated by the S119 residue.[50]

Possible effects of the mutations on the structure of CYP3A4 are illustrated in Figure 8, which shows the largest clusters obtained in simulations with two CBZ molecules of wild-type CYP3A4 and mutants I369F and A370V compared to the X-ray crystal structure of CYP3A4 with metyrapone (PDB: 1W0G).[18] The $\pi-\pi$ stacking interactions between residues F316 and F367 that are also found in most X-ray structures are likely to be structurally important. The residues I369 and A370 reside in the 1.4 K β loop (residues 368−372) that connects the α helix

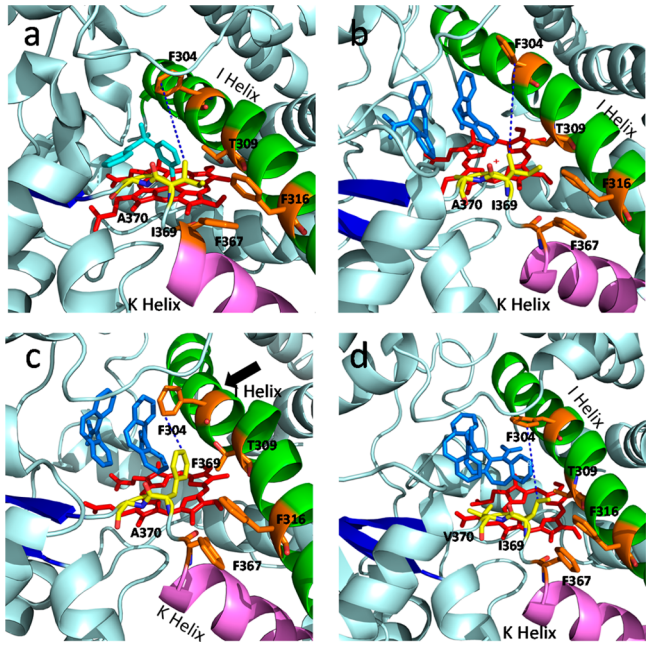

Figure 8. Comparison of the X-ray structure of CYP3A4 (PDB: 1W0G) with the simulated structure cluster representatives. (a) Active site of CYP3A4 structure with metyrapone (light blue) bound.[18] (b−d) Cluster representatives of MD simulations of (b) CYP3A4 wild-type and mutants (c) I369F and (d) A370V with two CBZ molecules (marine blue). Residues F316 and F367 (orange) apparently engage in $\pi-\pi$ stacking interactions. The 1.4 K/β loop (consisting of residues 368−372 (PIAMR) that join the K helix (violet) to the sequential β sheet (blue)) makes Van der Waals contacts with the long I helix (green). Mutated residues are shown in yellow. Note: in panel c, the bulky phenylalanine in the I369F mutant projects into the active site, reducing the accessibility of the heme. Over the length of one simulation of the I369F mutant, the I helix exhibits a kink (black arrow) around residue F304 that additionally restricts access to the active site because of a dramatic decrease in the distance between the side-chains of F304 and residue 369 (blue dashes). The average distances over the total simulation time are (b) $\Delta_{SC(WT)} \approx 11.6$ Å in wild-type CYP3A4, (c) $\Delta_{SC(I369F)} \approx 8.0$ Å in the I369F mutant, and (d) $\Delta_{SC(A370V)} \approx 13.0$ Å in the A370V mutant.

K (violet) with the subsequent β strand (blue) and adjoins the active site in Van der Waals contact to the α helix I (green). The structural changes upon substitution of phenylalanine at I369 are apparently important for the increased substrate inhibition observed in the I369F mutant (Figure 5, Table 1). The substitution at I369 with phenylalanine (or leucine) is likely to affect hydrophobic interactions in the active site, thereby promoting inhibitory substrate-binding and/or steric or conformational effects. The I369F substitution may reduce the volume of the active site and concomitantly restrict access to the heme (Figure 8c). The bulky phenylalanine residue 369 in the vicinity of the heme is likely to destabilize the ligation of the water molecule in the low-spin P450 state and to be the source of the observed increase in the proportion of high-spin P450 in the substrate-free I369F mutant (Figure 4). The I369F substitution may reduce the empty space between the 1.4 K/β loop and helix I that face each other in the active site. An analysis of the trajectories of residues F304 and 369 in the MD simulations (Figure S2) reveals a decrease of the mean distance between the side chains of these residues (blue dashes in Figure 8b−d) from ~11.6 Å in wild-type CYP3A4 ($\Delta_{SC(WT)}$, Figures 8b and S2) to ~8.0 Å in I369F ($\Delta_{SC(I369F)}$, Figures 8c and S2)

DOI: 10.1021/bi5011656
Biochemistry 2015, 54, 711−721

on average over the total simulation; the corresponding distance in the A370V mutant was ~13.0 Å ($\Delta_{SC(A370V)}$, Figures 8d and S2). The formation of a kink in the helix near the F304 residue (Figure 8c, black arrow) may further restrict access to the active site in the I369F mutant: this conformational change was, however, seen in only one out of five simulations. Furthermore, although not revealed in the simulations, a direct interaction of the I369F phenylalanine with residue F304 may be possible and contribute to the changes in the kinetics observed with this mutant. In the I369L mutant, the side-chain γ-methyl groups of leucine may more closely interact with the T309 side chain to move the 1.4 K/β loop and to induce a similar conformational change in helix I as seen in the simulation of the I369F mutant. A direct effect of the leucine on the accessibility to the heme may also be plausible.

Stabilization of substrate binding by the additional phenylalanine residue near the heme moiety in the I369F mutant via stacking interactions of the aromatic rings may contribute to the high rate of CBZ turnover observed with this mutant at low CBZ concentrations. At higher CBZ concentrations, the presence of several CBZ molecules stacked on top of each other above the heme may prevent dissociation of product and be responsible for the observed substrate inhibition (Table 1).

Elimination of substrate inhibition in mutants A370V and A370L (Figure 5, Table 1) is associated with a significant increase in the S_{50} value for these mutants as compared to that of wild-type, and the decreased affinity for CBZ provides further support for the importance of the K/β-loop region for CBZ binding. It seems plausible that the steric clashes between the larger aliphatic side chains of the valine and leucine of these mutants and the metabolized or stabilizing CBZ molecule may destabilize the substrate stacking, which is hypothesized to be responsible for substrate inhibition.

The observation that the mutants with higher affinities for CBZ display more pronounced substrate inhibition provides additional support for the above hypothesis that the mechanism of substrate inhibition is due to the binding of additional CBZ molecules that impede the egress of product. In contrast, the finding that the mutants with lower affinities for CBZ exhibit homotropic cooperativity is consistent with the stabilization of the catalytically competent enzyme–substrate complex upon binding of a second CBZ. Whether these correlations are specific to metabolism of CBZ or represent a general characteristic of CYP3A4-catalyzed reactions requires further experimentation.

In view of our original goal to generate CYP3A4 variants for use in biosensors capable of detecting CBZ, one may argue that the A370V variant is the best candidate because it exhibits the highest maximal rate of CBZ turnover of all the probed enzyme variants. However, taking into account that the target therapeutic concentrations of CBZ in blood plasma are limited to the range of 17 to 70 μM,[7] we may conclude that the decreased affinity of A370V for CBZ (S_{50} = 1.1 mM) undermines its practical utility. In our view, the most promising enzyme variant for practical use is I369F, where the rate of CBZ turnover is increased 2-fold and the S_{50} value obtained with the use of eq 2 remains unaffected (Table 1). However, it should be taken into account that the rate of substrate turnover and the utilization of the reducing equivalents by the enzyme do not necessarily obey a strict proportionality. Baas et al. showed that the consumption of NADPH as a source of reducing equivalents for CYP3A4 reaches its maximum at substrate concentrations that are subsaturating for the enzymatic turnover of testosterone.[51] Furthermore, the actual relationships between the faradaic current to the electrodes and the enzyme turnover may differ between the mutants. Therefore, further assessment of the potential utility of the generated CYP3A4 variants for the use in CBZ sensors requires investigations with the enzyme immobilized on the electrode surface.

Determination of the crystal structures of the CYP3A4 variants investigated in this study, such as I369F and S119A, would be expected to yield important insights regarding the relevance of structural aspects to mechanisms of substrate inhibition and homotropic cooperativity in CYP3A4. In spite of the structural plasticity of CYP3A4,[47,52] we have been able to use MD simulations to identify plausible productive and nonproductive binding modes for one or more substrate molecules in the substrate-binding pocket of the enzyme. In particular, the combination of MD simulations and pose clustering to guide site-directed mutagenesis has resulted in the design of enzyme variants that exhibit altered functional properties, such as homotropic cooperativity, substrate inhibition, and substrate affinities, *in vitro*. This approach may prove to be generally applicable to other enzyme–substrate pairs as a means to probe binding interactions and mechanisms and to modulate functionality.

■ ASSOCIATED CONTENT

Supporting Information

Information regarding selection and suggestion of mutants, COM tables, equation derivation steps, distances of the CBZ C10,11 COM to the heme iron in MD simulations, and time series data of the distance between the center of the C10–C11 bond in CBZ and the heme iron and between the side chains of residue 369 and Phe304. This material is available free of charge via the Internet at http://pubs.acs.org.

■ AUTHOR INFORMATION

Corresponding Authors

*D.R.D.: Telephone: +1-559-751-2309. E-mail: dmrdavyd@gmail.com.

*A.C.: Telephone: +41-44-635-5521. E-mail: caflisch@bioc.uzh.ch.

*W.H.K.: Telephone: +41-44-632-2875. E-mail: koppenol@inorg.chem.ethz.ch.

Present Addresses

P.L.B.: Foundation for Research on Information Technologies in Society (IT'IS), Zeughausstrasse 43, CH-8004 Zurich, Switzerland.

J.R.H.: School of Pharmacy, University of Connecticut, Storrs, Connecticut 06269 United States.

Funding

This research was supported in part by grant GM054995 from the National Institutes of Health (J.R.H.), grant 315230_149897 from the Swiss National Science Foundation (A.C.), Sinergia grant 127547 of the Swiss National Science Foundation (U.M), and the Swiss Federal Institute of Technology (W.H.K.).

Notes

The authors declare no competing financial interest.

DOI: 10.1021/bi5011656
Biochemistry 2015, 54, 711–721

■ ACKNOWLEDGMENTS

We thank Michael Fairhead, Michael Richter, and Linda Thöny for their valued support of C.M. in experimental molecular biology techniques. We thank Marino Convertino for help with the simulation setup and protocols in the initial phase of this project. We thank Antonio Baici for instrumental comments on initial interpretation of the kinetics. C.M. thanks Alexandra Dolder for technical assistance in preparation and analysis of the proteins.

■ ABBREVIATIONS

CBZ, carbamazepine (5*H*-dibenzo[*b*,*f*]azepine-5-carboxamide); CHAPS, 3-[(3-cholamidopropyl)dimethylammonio]-1-propanesulfonate; COM, center of mass; CYP3A4, cytochrome P450 3A4; CYPOR, cytochrome P450 oxidoreductase; MD, molecular dynamics; rCYP3A4, reconstituted (recombinant) CYP3A4

■ REFERENCES

(1) Shimada, T., Yamazaki, H., Mimura, M., Inui, Y., and Guengerich, F. P. (1994) Interindividual variants in human liver cytochrome-P-450 enzymes involved in the oxidation of drugs, carcinogens and toxic chemicals: studies with liver-microsomes of 30 Japanese and 30 Caucasians. *J. Pharmacol. Exp. Ther. 270*, 414−423.

(2) Guengerich, F. P. (1999) Cytochrome P-450 3A4: Regulation and role in drug metabolism. *Annu. Rev. Pharmacol. Toxicol. 39*, 1−17.

(3) Pearce, R. E., Vakkalagadda, G. R., and Leeder, J. S. (2002) Pathways of carbamazepine bioactivation *in vitro* I. Characterization of human cytochromes P450 responsible for the formation of 2- and 3-hydroxylated metabolites. *Drug Metab. Dispos. 30*, 1170−1179.

(4) Kerr, B. M., Thummel, K. E., Wurden, C. J., Klein, S. M., Kroetz, D. L., Gonzalez, F. J., and Levy, R. (1994) Human liver carbamazepine metabolism: Role of CYP3A4 and CYP2C8 in 10,11-epoxide formation. *Biochem. Pharmacol. (Amsterdam, Neth.) 47*, 1969−1979.

(5) Nakamura, H., Nakasa, H., Ishii, I., Ariyoshi, N., Igarashi, T., Ohmori, S., and Kitada, M. (2002) Effects of endogenous steroids on CYP3A4-mediated drug metabolism by human liver microsomes. *Drug Metab. Dispos. 30*, 534−540.

(6) Nakamura, H., Torimoto, N., Ishii, I., Ariyoshi, N., Nakasa, H., Ohmori, S., and Kitada, M. (2003) CYP3A4 and CYP3A7-mediated carbamazepine 10,11-epoxidation are activated by differential endogenous steroids. *Drug Metab. Dispos. 31*, 432−438.

(7) Egnell, A.-C., Houston, B., and Boyer, S. (2003) In vivo CYP3A4 heteroactivation is a possible mechanism for the drug interaction between felbamate and carbamazepine. *J. Pharmacol. Exp. Ther. 305*, 1251−1262.

(8) Egnell, A.-C., Houston, J. B., and Boyer, C. S. (2005) Predictive models of CYP3A4 heteroactivation: *In vitro*−*in vivo* scaling and pharmacophore modeling. *J. Pharmacol. Exp. Ther. 312*, 926−937.

(9) Maekawa, K., Yoshimura, T., Saito, Y., Fujimura, Y., Aohara, F., Emoto, C., Iwasaki, K., Hanioka, N., Narimatsu, S., Niwa, T., and Sawada, J. (2009) Functional characterization of CYP3A4.16: Catalytic activities toward midazolam and carbamazepine. *Xenobiotica 39*, 140−147.

(10) Torimoto, N., Ishii, I., Hata, M., Nakamura, H., Imada, H., Ariyoshi, N., Ohmori, S., Igarashi, T., and Kitada, M. (2003) Direct interaction between substrates and endogenous steroids in the active site may change the activity of cytochrome P450 3A4. *Biochemistry 42*, 15068−15077.

(11) Ueng, Y.-F., Kuwabara, T., Chun, Y.-J., and Guengerich, F. P. (1997) Cooperativity in oxidations catalyzed by cytochrome P450 3A4. *Biochemistry 36*, 370−381.

(12) Korzekwa, K. R., Krishnamachary, N., Shou, M., Ogai, A., Parise, R. A., Rettie, A. E., Gonzalez, F. J., and Tracy, T. S. (1998) Evaluation of atypical cytochrome P450 kinetics with two-substrate models: Evidence that multiple substrates can simultaneously bind to cytochrome P450 active sites. *Biochemistry 37*, 4137−4147.

(13) Houston, J. B., and Kenworthy, K. E. (2000) *In vitro*−*in vivo* scaling of CYP kinetic data not consistent with the classical Michaelis−Menten model. *Drug Metab. Dispos. 28*, 246−254.

(14) Yacobi, A., Zlotnick, S., Colaizzi, J. L., Moros, D., Masson, E., Abolfathi, Z., LeBel, M., Mehta, R., Golander, Y., and Levitt, B. (1999) A multiple-dose safety and bioequivalence study of a narrow therapeutic index drug: A case for carbamazepine. *Clin. Pharmacol. Ther. (N.Y., NY, U.S.) 65*, 389−394.

(15) Bistolas, N., Wollenberger, U., Jung, C., and Scheller, F. W. (2005) Cytochrome p450 biosensors−a review. *Biosens. Bioelectron. 20*, 2408−2423.

(16) Dodhia, V. R., Sassone, C., Fantuzzi, A., Nardo, G. D., Sadeghi, S. J., and Gilardi, G. (2008) Modulating the coupling efficiency of human cytochrome P450 CYP3A4 at electrode surfaces through protein engineering. *Electrochem. Commun. 10*, 1744−1747.

(17) Krishnan, S., Wasalathanthri, D., Zhao, L., Schenkman, J. B., and Rusling, J. F. (2011) Efficient bioelectronic actuation of the natural catalytic pathway of human metabolic cytochrome P450s. *J. Am. Chem. Soc. 133*, 1459−1465.

(18) Williams, P. A., Cosme, J., Vinković, D. M., Ward, A., Angove, H. C., Day, P. J., Vonrhein, C., Tickle, I. J., and Jhoti, H. (2004) Crystal structures of human cytochrome P450 3A4 bound to metyrapone and progesterone. *Science 305*, 683−686.

(19) Brooks, B. R., Brooks, C. L., Mackerell, A. D., Nilsson, L., Petrella, R. J., Roux, B., Won, Y., Archontis, G., Bartels, C., Boresch, S., Caflisch, A., Caves, L., Cui, Q., Dinner, A. R., Feig, M., Fischer, S., Gao, J., Hodoscek, M., Im, W., Kuczera, K., Lazaridis, T., Ma, J., Ovchinnikov, V., Paci, E., Pastor, R. W., Post, C. B., Pu, J. Z., Schaefer, M., Tidor, B., Venable, R. M., Woodcock, H. L., Wu, X., Yang, W., York, D. M., and Karplus, M. (2009) CHARMM: The biomolecular simulation program. *J. Comput. Chem. 30*, 1545−1614.

(20) MacKerell, A. D., Feig, M., and Brooks, C. L. (2003) Improved treatment of the protein backbone in empirical force fields. *J. Am. Chem. Soc. 126*, 698−699.

(21) Foloppe, N., Sagemark, J., Nordstrand, K., Berndt, K. D., and Nilsson, L. (2001) Structure, dynamics and electrostatics of the active site of glutaredoxin 3 from *Escherichia coli*: Comparison with functionally related proteins. *J. Mol. Biol. 310*, 449−470.

(22) Vanommeslaeghe, K., Hatcher, E., Acharya, C., Kundu, S., Zhong, S., Shim, J., Darian, E., Guvench, O., Lopes, P., Vorobyov, I., and Mackerell, A. D. (2010) CHARMM general force field: A force field for drug-like molecules compatible with the CHARMM all-atom additive biological force fields. *J. Comput. Chem. 31*, 671−690.

(23) Vanommeslaeghe, K., and MacKerell, A. D. (2012) Automation of the CHARMM general force field (CGenFF) I: Bond perception and atom typing. *J. Chem. Inf. Model. 52*, 3144−3154.

(24) Vanommeslaeghe, K., Raman, E. P., and MacKerell, A. D. (2012) Automation of the charmm general force field (CGenFF) II: Assignment of bonded parameters and partial atomic charges. *J. Chem. Inf. Model. 52*, 3155−3168.

(25) van der Spoel, D., Lindahl, E., Hess, B., Groenhof, G., Mark, A. E., and Berendsen, H. J. C. (2005) GROMACS: Fast, flexible, and free. *J. Comput. Chem. 26*, 1701−1718.

(26) Jorgensen, W. L., Chandrasekhar, J., Madura, J. D., Impey, R. W., and Klein, M. L. (1983) Comparison of simple potential functions for simulating liquid water. *J. Chem. Phys. 79*, 926−935.

(27) Darden, T., York, D., and Pedersen, L. (1993) Particle mesh Ewald: An *N*·log(*N*) method for Ewald sums in large systems. *J. Chem. Phys. 98*, 10089−10092.

(28) Hess, B., Bekker, H., Berendsen, H. J. C., and Fraaije, J. G. E. M. (1997) LINCS: A linear constraint solver for molecular simulations. *J. Comput. Chem. 18*, 1463−1472.

(29) Bussi, G., Donadio, D., and Parrinello, M. (2007) Canonical sampling through velocity rescaling. *J. Chem. Phys. 126*, 14101−14107.

(30) Parrinello, M., and Rahman, A. (1981) Polymorphic transitions in single crystals: A new molecular dynamics method. *J. Appl. Phys. 52*, 7182−7190.

(31) Nosé, S., and Klein, M. L. (1983) Constant pressure molecular dynamics for molecular systems. *Mol. Phys. 50*, 1055−1076.

DOI: 10.1021/bi5011656
Biochemistry 2015, 54, 711−721

(32) (2014) *The PyMOL Molecular Graphics System*, version 1.5.0.4; Schrödinger, LLC: Camberley, U.K. http://www.pymol.org/
(33) Seeber, M., Cecchini, M., Rao, F., Settanni, G., and Caflisch, A. (2007) Wordom: A program for efficient analysis of molecular dynamics simulations. *Bioinformatics 23*, 2625−2627.
(34) Vitalis, A., and Caflisch, A. (2012) Efficient construction of mesostate networks from molecular dynamics trajectories. *J. Chem. Theory Comput. 8*, 1108−1120.
(35) Vitalis, A., and Pappu, R. V. (2009) Methods for Monte Carlo simulations of biomacromolecules. *Annu. Rep. Comput. Chem. 5*, 49−76.
(36) Harlow, G. R., and Halpert, J. R. (1997) Alanine-scanning mutagenesis of a putative substrate recognition site in human cytochrome P450 3A4: role of residues 210 and 211 in flavonoid activation and substrate specificity. *J. Biol. Chem. 272*, 5396−5402.
(37) Omura, T., and Sato, R. (1964) Carbon monoxide-binding pigment of liver microsomes: II. Solubilization, purification, and properties. *J. Biol. Chem. 239*, 2379−&.
(38) Tsalkova, T. N., Davydova, N. Y., Halpert, J. R., and Davydov, D. R. (2007) Mechanism of interactions of alpha-naphthoflavone with cytochrome P450 3A4 explored with an engineered enzyme bearing a fluorescent probe. *Biochemistry 46*, 106−119.
(39) Davydov, D. R., Sineva, E. V., Sistla, S., Davydova, N. Y., Frank, D. J., Sligar, S. G., and Halpert, J. R. (2010) Electron transfer in the complex of membrane-bound human cytochrome P450 3A4 with the flavin domain of P450BM-3: The effect of oligomerization of the heme protein and intermittent modulation of the spin equilibrium. *Biochim. Biophys. Acta, Bioenerg. 1797*, 378−390.
(40) Fernando, H., Davydov, D. R., Chin, C. C., and Halpert, J. R. (2007) Role of subunit interactions in p450 oligomers in the loss of homotropic cooperativity in the cytochrome P450 3A4 mutant L211F/D214E/F304W. *Arch. Biochem. Biophys. 460*, 129−140.
(41) French, J. S., and Coon, M. J. (1979) Properties of NADPH-cytochrome *P*-450 reductase purified from rabbit liver microsomes. *Arch. Biochem. Biophys. 195*, 565−577.
(42) Davydov, D. R., Deprez, E., Hui Bon Hoa, G., Knyushko, T. V., Kuznetsova, G. P., Koen, Y. M., and Archakov, A. I. (1995) High-pressure-induced transitions in microsomal cytochrome P450 2B4 in solution: Evidence for conformational inhomogeneity in the oligomers. *Arch. Biochem. Biophys. 320*, 330−344.
(43) Khan, K. K., He, Y. Q., Domanski, T. L., and Halpert, J. R. (2002) Midazolam oxidation by cytochrome P450 3A4 and active-site mutants: An evaluation of multiple binding sites and of the metabolic pathway that leads to enzyme inactivation. *Mol. Pharmacol. 61*, 495−506.
(44) He, Y. A., He, Y. Q., Szklarz, G. D., and Halpert, J. R. (1997) Identification of three key residues in substrate recognition site 5 of human cytochrome P450 3A4 by cassette and site-directed mutagenesis. *Biochemistry 36*, 8831−8839.
(45) Kumar, S., Davydov, D. R., and Halpert, J. R. (2005) Role of cytochrome B_5 in modulating peroxide-supported CY3A4 activity: Evidence for a conformational transition and cytochrome P450 heterogeneity. *Drug Metab. Dispos. 33*, 1131−1136.
(46) Sevrioukova, I. F., and Poulos, T. L. (2013) Understanding the mechanism of cytochrome P450 3A4: Recent advances and remaining problems. *Dalton Trans. 42*, 3116−3126.
(47) Ekroos, M., and Sjögren, T. (2006) Structural basis for ligand promiscuity in cytochrome P450 3A4. *Proc. Natl. Acad. Sci. U.S.A. 103*, 13682−13687.
(48) Sevrioukova, I. F., and Poulos, T. L. (2010) Structure and mechanism of the complex between cytochrome P4503A4 and ritonavir. *Proc. Natl. Acad. Sci. U.S.A. 107*, 18422−18427.
(49) Park, H., Lee, S., and Suh, J. (2005) Structural and dynamical basis of broad substrate specificity, catalytic mechanism, and inhibition of cytochrome P450 3A4. *J. Am. Chem. Soc. 127*, 13634−13642.
(50) Sevrioukova, I. F., and Poulos, T. L. (2013) Dissecting cytochrome P450 3A4−ligand interactions using ritonavir analogues. *Biochemistry 52*, 4474−4481.
(51) Baas, B. J., Denisov, I. G., and Sligar, S. G. (2004) Homotropic cooperativity of monomeric cytochrome P450 3A4 in a nanoscale native bilayer environment. *Arch. Biochem. Biophys. 430*, 218−228.
(52) Sineva, E. V., Rumfeldt, J. A. O., Halpert, J. R., and Davydov, D. R. (2013) A large-scale allosteric transition in cytochrome P450 3A4 revealed by luminescence resonance energy transfer (LRET). *PLoS One 8*, e83898.

DOI: 10.1021/bi5011656
Biochemistry 2015, 54, 711−721